Subfemtosecond hybrid synchronization between ultrafast Yb and Er fiber laser systems by controlling the relative injection timing

Bo-Wei Tsai,[1] Shang-Ying Wu,[2] Chieh Hu,[3] Wei-Wei Hsiang,[1,*] and Yinchieh Lai[2,4]

[1]*Department of Physics, Fu Jen Catholic University, Taipei 24205, Taiwan*

[2]*Department of Photonics & Institute of Electro-Optical Engineering, National Chiao-Tung University, Hsinchu 30010, Taiwan*

[3]*Additive Manufacturing & Laser Application Technology Center, ITRI South Campus, Tainan 73445, Taiwan*

[4]*Research Center for Applied Sciences, Academia Sinica, Taipei 11529, Taiwan*

**Corresponding author: 069179@mail.fju.edu.tw*

Received May 2, 2013; revised July 21, 2013; accepted August 6, 2013;
posted August 8, 2013 (Doc. ID 189903); published August 30, 2013

We report experimental as well as theoretical investigation of the key factors that influence the relative timing jitter between hybrid synchronized ultrafast Yb and Er fiber laser systems. Experimental results show that, within the achievable synchronization range, the synchronization performance varies significantly with the relative injection timing between the 1 μm master and 1.5 μm slave pulses. This observation is in agreement with the insights obtained from the theoretical analysis, which identifies the retiming effect as a function of the initial condition of the master–slave pulse collision. By controlling the relative injection timing with a low-bandwidth intracavity feedback, relative timing jitter as low as 0.87 fs (within 1.9 MHz bandwidth) is successfully obtained.

OCIS codes: (320.7090) Ultrafast lasers; (140.4050) Mode-locked lasers; (140.3510) Lasers, fiber; (320.7110) Ultrafast nonlinear optics.

http://dx.doi.org/10.1364/OL.38.003456

Optical pulse timing synchronization is a crucial step for developing new techniques in ultrafast science and technology. Some important examples include time-resolved imaging and spectroscopy, fs optical parametric amplifiers (OPA), and coherent pulse synthesis, as well as precise timing distribution [1–3]. Both the passive and active synchronization techniques have been actively explored to lock the repetition rates of two ultrashort pulse lasers. In active synchronization schemes, complicated setups of precise pulse timing detection and high-speed intracavity feedback are typically required for achieving low timing jitters [4,5]. In contrast, the passive synchronization schemes based on the shared cavity or pulse injection configuration can take advantage of the instantaneity of the nonlinear optical cross-phase modulation (XPM) to implement a high-speed synchronization feedback [6–8]. As a further extension, it is expected that passive synchronization assisted by a low-bandwidth intracavity feedback should be able to suppress the fast timing fluctuations as well as remove the slow timing drifts. The scheme should be capable of achieving long-term sub-fs synchronization with low-cost feedback devices. However, such a hybrid synchronization approach with sub-fs precision was only demonstrated on the solid-state lasers [7]. For ultrafast fiber laser systems, it is still a challenge to obtain sub-fs synchronization by the hybrid synchronization technique [6,8].

In this Letter, we report experimental as well as theoretical investigation of the key factors that influence the relative timing jitter between the 1 μm Yb and 1.5 μm Er fiber laser systems synchronized by the pulse injection technique and with a low-bandwidth intracavity feedback. It is found experimentally that the synchronization performance can vary significantly with respect to the relative injection timing between the 1 μm master and 1.5 μm slave pulses. A simple theoretical analysis based on the linearized evolution equations of the laser pulse parameters has also been derived to examine the effects of the two-color pulse collision on the retiming force for achieving synchronization. By controlling the relative injection timing with a low-bandwidth intracavity feedback, such that the slave pulse experiences the maximum retiming force, a relative timing jitter as low as 0.87 fs (1.9 MHz bandwidth) between the two-color ultrafast fiber laser systems can be obtained.

Figure 1 shows the experimental setup of the hybrid synchronization between the fs Yb and Er fiber laser amplifier systems with the pulse repetition rates of ~43.28 MHz. The homebuilt mode-locked Er fiber and Yb fiber lasers are both based on the nonlinear polarization rotation technique, and their output pulses

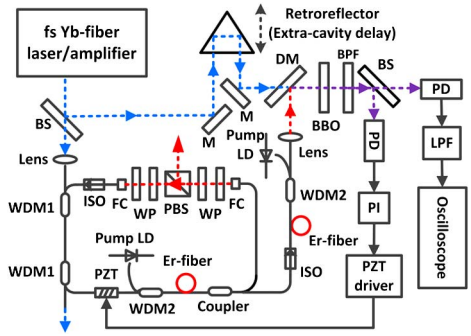

Fig. 1. Experimental setup of the hybrid synchronized Er and Yb fiber laser amplifier systems. BS, beam splitter; DM, dichroic mirror; BPF, optical bandpass filter; PD, photodiode; LPF, electric low-pass filter; PI, proportional-integral controller; PZT, piezoelectric transducer; M, mirror; WDM, wavelength division multiplexer (WDM1, 1560/1030 nm; WDM2, 1560/976 nm); LD, laser diode; ISO, polarization independent isolator; PBS, polarization beam splitter; FC, fiber collimator; WP, wave plates.

are amplified by the single-cladding Er-doped (OFS EDF 80) and double-cladding Yb-doped (LIEKKI, Yb1200-10/125DC) fiber amplifiers, respectively. The net intracavity dispersions of the stretched pulse Er fiber and self-similar Yb fiber lasers are ~ -0.023 ps^2 and ~ 0.011 ps^2, respectively. The anomalous intracavity dispersion of the Er fiber laser is required for being a slave laser in the passive synchronization scheme. After amplification the 1.5 μm pulses are compressed by the single-mode fiber (SMF 28) to ~70 fs with the pulse energy of 1.5 nJ. For the 1 μm amplified pulses, dechirp is achieved by the transmission grating pair (1000 lines/mm) and, after compression, the pulse energy of 9 nJ and pulse duration of ~110 fs can be obtained. The hybrid synchronization procedures begin with the injection of a small part of the output power of the Yb laser amplifier system into the slave Er fiber laser via the two wavelength division multiplexers (WDM1). The remaining of the 1 μm output is combined with the 1.5 μm pulses from the Er fiber laser amplifier system to be incident on a nonlinear BBO crystal. Within a suitable range of the extracavity delay between the 1 μm master and 1.5 μm slave pulses, the sum-frequency generation (SFG) signals can be generated and used for the measurement of the timing jitter as well as for the intracavity feedback control. The feedback loop consists of a proportional-integral controller and a piezoelectric transducer (PZT) driver, and the cavity length of the Er fiber laser is adjusted by the PZT wound with SMF 28. By locking the SFG signals at the middle height of the cross correlation trace, the slow timing drift, which is the main characteristic of the passive synchronization under the environmental perturbations, can be effectively removed. The bandwidth of the intracavity feedback of the PZT servo is less than 3 kHz, and the measurement bandwidth of the relative timing jitter is determined by the low-pass filter of 1.9 MHz. It should be noted that, because the extracavity time separation between the 1 and 1.5 μm pulses is fixed by the feedback loop, the detuning of the extracavity delay via the retroreflector (see Fig. 1) will, accordingly, change the relative injection timing between the two color pulses inside the Er fiber laser [9].

Although the hybrid synchronization can be achieved over a wide range of the extracavity delay, we find that the corresponding relative timing jitter may vary significantly. This reveals that the relative injection timing between the master and slave pulses inside the Er fiber laser can affect the synchronization performance. Figure 2(a) demonstrates the successful locking of the relative pulse timing with the turn-on of the feedback. Figure 2(b) shows the measurement results of the cross correlation trace and the minimum relative timing jitter obtained by optimizing the position (offset is 40 μm) of the extracavity delay with the injection power of 30 mW. The amplitude-to-time conversion ratio near the middle height of the cross correlation trace is 14.75 fs/V, and the amplitude fluctuation of 58.91 mV in Fig. 2(b) corresponds to the relative timing jitter of 0.87 fs. When the offset position of the extracavity delay is moved from 40 to 160 μm, as shown in the inset of Fig. 2(b), the amplitude fluctuation and its corresponding timing jitter are increased to 129.2 mV and 1.91 fs, respectively. Within all the locking range of the hybrid synchronization, the

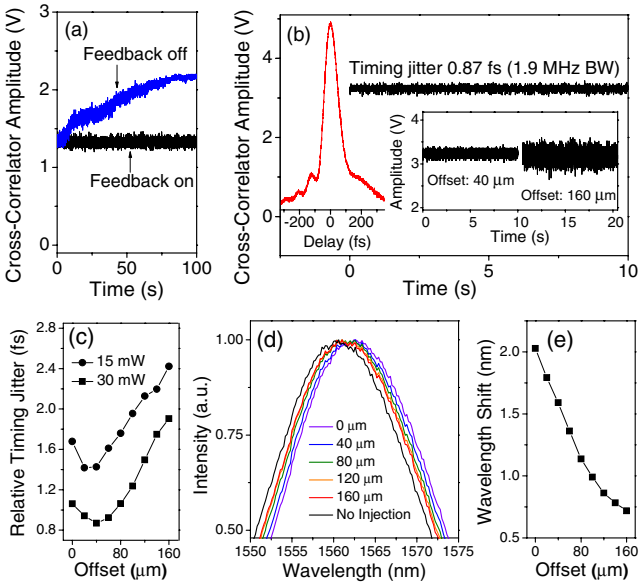

Fig. 2. (a) Demonstration of successful feedback; (b) measured cross correlation trace and the timing jitters; (c) measured timing jitters of the slave Er fiber laser with different extracavity delay and injection power of 15 and 30 mW; (d) measured optical spectra of the slave Er fiber laser with different extracavity delay and injection power of 30 mW; (e) shift of the center wavelength versus the distance offset.

relative timing jitter measured with respect to different extracavity delays for the two injection powers of 15 and 30 mW are shown in Fig. 2(c). Besides the effects from the extracavity delay, it can be seen that the relative timing jitter measured from the 30 mW injection power is smaller than those obtained from the 15 mW injection power. An injection power higher than 30 mW has been tried to get an even smaller relative timing jitter. However, the instability of the mode-locking of the Er fiber laser prevents the better synchronization performance from being obtained, possibly due to the excess nonlinear polarization rotation introduced by the 1 μm injection pulse. In addition to the relative timing jitter, the optical spectra of the slave Er fiber laser are also measured concurrently with the different delays for the case of the 30 mW injection power, as shown in Fig. 2(d). Compared to the free-running spectrum of the mode-locked Er fiber laser, only redshift of the center wavelength can be observed in our hybrid synchronization experiment, as also shown in Fig. 2(e).

Besides the time domain measurement of the relative timing jitter, the frequency domain analysis has been performed as well to identify the timing jitter suppression originating from the active or passive synchronization mechanisms. To achieve this, the cross correlation signal under the hybrid synchronization is connected to an rf spectrum analyzer (Agilent E4402B with UKB), and Fig. 3 shows the power spectrum density (PSD) of the cross correlation output with respect to different frequency ranges. The blue (bottom) curve of Fig. 3(a) is the measurement result under the stable hybrid synchronization. When the gain of the PI servo exceeds the stable value, obvious oscillations appearing around 3 kHz can be seen from the green (middle with three large peaks) curve in Fig. 3(a). Therefore the bandwidth of the active

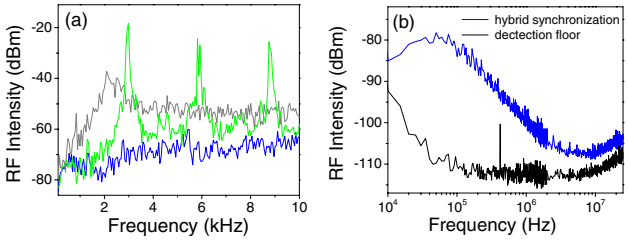

Fig. 3. Frequency domain analysis of the cross correlation output under the hybrid synchronization. (a) Blue curve (bottom): the stable hybrid synchronization; green curve (middle): the hybrid synchronization with an excess gain of the PI servo; gray curve (top): the hybrid synchronization with only 2.5 mW injection power. (b) Blue curve (top): the stable hybrid synchronization; black curve (bottom): the detection floor.

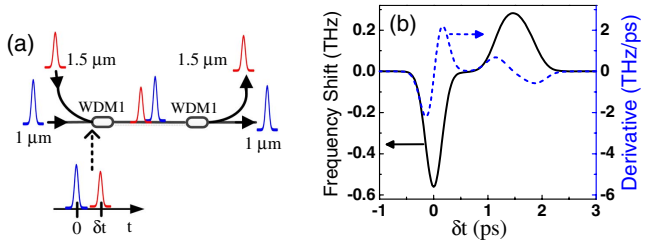

Fig. 4. (a) Schematic illustration of the two-color pulse collision; (b) calculated single-pass XPM-induced frequency shift and its first-order derivative versus the relative position between the master and slave pulses when entering the SMF of 0.9 m.

synchronization is less than 3 kHz. The gray (top) curve in Fig. 3(a) shows the case with a relative timing jitter of ~10 fs when the 1 μm injection power (~2.5 mW) is almost completely blocked. It indicates that, for frequencies above 1 kHz, passive synchronization plays the dominant role to suppress the relative timing jitter. The PSD of the cross correlation output from 10 kHz to the Nyquist frequency (21.6 MHz) is measured by using another detector with a broader bandwidth, as shown in Fig. 3(b). Above 100 kHz, the slope of the PSD, i.e., the blue (top) curve in Fig. 3(b), begins to decay with a slope close to $1/f^2$, which exhibits the typical timing jitter characteristics of mode-locked fiber lasers [10,11]. This means that the locking bandwidth of the passive synchronization should be at least 100 kHz in our experiment. Moreover, like other mode-locked fiber lasers, the part of the PSD with a frequency higher than a few MHz will not contribute significantly to the overall integrated relative timing jitter. Although the detection floor, the black (bottom) curve in Fig. 3(b), is much lower than the PSD of the cross correlation output, the measurement resolution of the relative timing jitter is mainly limited by the amplitude noise of the SFG signal itself, which corresponds to ~0.35 fs in our experiment.

The theoretical analysis aimed to clarify the above experimental observations has also been carried out. First of all, the net XPM-induced frequency shift from the master–slave pulse collision in the common fiber section is numerically calculated with respect to the different injection timing. The effect serves as a retiming force on the slave Er fiber laser for achieving synchronization. The theoretical model is based on the coupled nonlinear Schrödinger equation, and the numerical method of fourth-order Runge–Kutta in the interaction picture (RK4IP [12]) are utilized to obtain the net single-pass XPM-induced frequency shift as well as its first-order derivative with respect to the timing separation between the slave and master pulses when they enter the copropagation fiber section, as illustrated in Fig. 4(a). The obtained results are shown in Fig. 4(b). The parameters used in the simulation are estimated to be close to the actual experimental condition (fiber length: 0.9 m, 1.5 μm; pulse: 300 fs, 0.2 nJ; 1 μm pulse: 200 fs, 0.74 nJ; GVD: 23 ps^2/km at 1 μm and −11 ps^2/km at 1.5 μm, respectively; nonlinear coefficient: 1.5 $W^{-1}\,km^{-1}$; pulse walk-off: −1.7 ps/m [9]). It can be clearly seen in Fig. 4(b) that, due to the GVD and pulse walk-off effects, the net single-pass XPM-induced frequency shift is not exactly antisymmetric and may lead to the experimental results in Fig. 2 when one examines the pulse dynamics of the slave Er fiber laser that acquires the retiming force from the successive collisions with the injection pulses.

The fluctuations of the timing position $\Delta t_{0,\mathrm{Er}}$ and center wavelength $\Delta\omega_{\mathrm{Er}}$ of the slave pulse can be described by the linearized evolution equations, similar to those of a typical active frequency-modulation mode-locked laser [13]:

$$T_R\frac{d\Delta\omega_{\mathrm{Er}}}{dT}=-\frac{4d_r}{3\tau^2}\Delta\omega_{\mathrm{Er}}+f'(\delta t)(\Delta t_{0,\mathrm{Er}}-\Delta t_{0,\mathrm{Yb}}),\quad(1)$$

$$T_R\frac{d\Delta t_{0,\mathrm{Er}}}{dT}=2d_i\Delta\omega_{\mathrm{Er}},\quad(2)$$

where d_r represents the gain bandwidth filtering effect, $f'(\delta t)$ denotes the first-order derivative of the net XPM-induced frequency shift at the equilibrium separation ($\delta t=\bar{t}_{0,\mathrm{Er}}-\bar{t}_{0,\mathrm{Yb}}$) between the master and slave pulse, τ is the pulse width, d_i is the GVD, $\Delta t_{0,\mathrm{Yb}}$ is the timing fluctuations of the injection pulse, T_R is the cavity round trip time, and T is on a time scale of the cavity round trip time. Here, for simplicity, we have ignored the noise sources of the Er fiber laser itself. The frequency response of the slave pulse's timing fluctuation $\Delta t_{0,\mathrm{Er}}$ to the injection pulse's timing fluctuation $\Delta t_{0,\mathrm{Yb}}$ can be easily obtained from solving Eqs. (1) and (2) in the frequency domain such that the power spectral density of the relative timing jitter can be expressed as [14]

$$\langle|\Delta t_{0,\mathrm{Er}}(\Omega)-\Delta t_{0,\mathrm{Yb}}(\Omega)|^2\rangle=\frac{\Omega^4+\left(\frac{4d_r\Omega}{3\tau^2T_R}\right)^2}{\left[\left(\Omega^2+\frac{2f'(\delta t)d_i}{T_R^2}\right)^2+\left(\frac{4d_r\Omega}{3\tau^2T_R}\right)^2\right]}\langle|\Delta t_{0,\mathrm{Yb}}(\Omega)|^2\rangle.\quad(3)$$

Equation (3) clearly indicates that the relative timing jitter can be reduced by increasing the value of $f'(\delta t)$, the first-order derivative of the net XPM-induced shift. Because the derivative value varies significantly with the relative injection timing δt, this explains why the relative timing jitter depends on the extracavity delay in our hybrid synchronization experiment. It is also in agreement with the observation that the minimum relative

timing jitter and stable hybrid synchronization are only accompanied by the redshift in the slave pulse's center wavelength. As shown in Fig. 4(b), the more stable synchronization range is the region with the larger positive first-order derivative $f'(\delta t)$, which corresponds to the region with the red (or negative) frequency shift $f(\delta t)$. The value of $f'(\delta t)$, as well as the current locking bandwidth of the passive synchronization in our experiment, is still lower than the fast PZT servo (~180 kHz) or an electro-optic modulator (> the Nyquist frequency) [2,15]. However, from the theoretical analysis presented above, the passive synchronization locking bandwidth can be increased without affecting the stable mode-locking by simultaneously shortening the copropagation fiber length and increasing the injection pulse energy.

The individual timing jitters of the mode-locked Er fiber and Yb fiber lasers in our experiment have not been characterized experimentally. According to their values of the intracavity dispersion, it is reasonable to estimate that individual timing jitters of the two fiber laser systems are within the fs range [10–11]. Nevertheless, due to the passive synchronization effect, i.e., the first term on the right hand side of Eq. (3), the sub-fs relative timing jitter can be obtained in our experiment. In [11] it was shown that the mode-locked fiber lasers with the close-to-zero intracavity dispersion are able to have the attosecond timing jitters. From Eq. (3), it is expected to obtain a lower relative timing jitter than our current results if the individual timing jitters of the master and slave fiber lasers can be further minimized by optimizing the intracavity dispersion. Recently, an alternative approach based on a single Er fiber laser with the two-branch amplifiers and highly nonlinear fibers has achieved an unprecedented synchronization accuracy with a 43-as relative timing jitter between the two-color pulses and demonstrated the successful synthesis of a single-cycle pulse [16,17]. Nevertheless, the synchronization techniques that directly lock the two ultrafast laser systems with different wavelengths are still needed, especially for the cases in which the wavelengths of the two-color pulses cannot be obtained simultaneously from supercontinuum generation in highly nonlinear fibers.

To conclude, we have experimentally and theoretically investigated the key factors that influence the timing jitter between two ultrafast fiber lasers synchronized by the pulse injection technique. By controlling the relative timing position between the injection and the slave pulses, an ultrasmall relative timing jitter of 0.87 fs (1.9 MHz bandwidth) between the Yb fiber and Er fiber fs lasers has been achieved. This hybrid synchronization scheme provides a very flexible configuration for the synchronization between two fiber laser systems as well as for the remote optical-to-optical timing distribution.

This work is supported by the National Science Council of Taiwan under the contracts NSC 99-2112-M-030-002-MY3 and NSC 99-2221-E-009-045-MY3 and by the ITRI South under the contract B200-101JE1. The authors also gratefully acknowledge the technical support from Dr. Jen-Long Peng.

References

1. S. Hädrich, J. Rothhardt, M. Krebs, S. Demmler, J. Limpert, and A. Tünnermann, Opt. Lett. **37**, 4910 (2012).
2. J. A. Cox, W. P. Putnam, A. Sell, A. Leitenstorfer, and F. X. Kärtner, Opt. Lett. **37**, 3579 (2012).
3. J. Kim, J. A. Cox, J. Chen, and F. X. Kärtner, Nat. Photonics **2**, 733 (2008).
4. R. K. Shelton, S. M. Foreman, L.-S. Ma, J. L. Hall, H. C. Kapteyn, M. M. Murnane, M. Notcutt, and J. Ye, Opt. Lett. **27**, 312 (2002).
5. T. R. Schibli, J. Kim, O. Kuzucu, J. T. Gopinath, S. N. Tandon, G. S. Petrich, L. A. Kolodziejski, J. G. Fujimoto, E. P. Ippen, and F. X. Kaertner, Opt. Lett. **28**, 947 (2003).
6. D. Yoshitomi, Y. Kobayashi, M. Kakehata, H. Takada, K. Torizuka, T. Onuma, H. Yokoi, T. Sekiguchi, and S. Nakamura, Opt. Lett. **31**, 3243 (2006).
7. D. Yoshitomi, Y. Kobayashi, H. Takada, M. Kakehata, and K. Torizuka, Opt. Lett. **30**, 1408 (2005).
8. D. Yoshitomi, X. Zhou, Y. Kobayashi, H. Takada, and K. Torizuka, Opt. Express **18**, 26027 (2010).
9. W.-W. Hsiang, W.-C. Chiao, C.-Y. Wu, and Y. Lai, Opt. Express **19**, 24507 (2011).
10. Y. Song, K. Jung, and J. Kim, Opt. Lett. **36**, 1761 (2011).
11. Y. Song, C. Kim, K. Jung, H. Kim, and J. Kim, Opt. Express **19**, 14518 (2011).
12. Z. Zhang, L. Chen, and X. Bao, Opt. Express **18**, 8261 (2010).
13. W.-W. Hsiang, H.-C. Chang, and Y. Lai, IEEE J. Quantum Electron. **46**, 292 (2010).
14. M. E. Grein, H. A. Haus, Y. Chen, and E. P. Ippen, IEEE J. Quantum Electron. **40**, 1458 (2004).
15. T. C. Briles, D. C. Yost, A. Cingöz, J. Ye, and T. R. Schibli, Opt. Express **18**, 9739 (2010).
16. F. Adler, A. Sell, F. Sotier, R. Huber, and A. Leitenstorfer, Opt. Lett. **32**, 3504 (2007).
17. G. Krauss, S. Lohss, T. Hanke, A. Sell, S. Eggert, R. Huber, and A. Leitenstorfer, Nat. Photonics **4**, 33 (2010).